Inverse identification of buffeting and self-excited wind loads on the hardanger bridge from acceleration data

Petersen, Oyvind W.; Øiseth, Ole; Nord, Torodd Skjerve; Lourens, Eliz-Mari

DOI
10.7712/120119.7238.20007

Publication date
2019

Document Version
Final published version

Published in
COMPDYN 2019: 7th ECCOMAS Thematic Conference on Computational Methods in Structural Dynamics and Earthquake Engineering

Citation (APA)
Petersen, O. W., Øiseth, O., Nord, T. S., & Lourens, E.-M. (2019). Inverse identification of buffeting and self-excited wind loads on the hardanger bridge from acceleration data. In M. Papadrakakis, & M. Fragiadakis (Eds.), *COMPDYN 2019: 7th ECCOMAS Thematic Conference on Computational Methods in Structural Dynamics and Earthquake Engineering* (pp. 4421-4433). (COMPDYN Proceedings; Vol. 3). https://doi.org/10.7712/120119.7238.20007

COMPDYN 2019
7th ECCOMAS Thematic Conference on
Computational Methods in Structural Dynamics and Earthquake Engineering
M. Papadrakakis, M. Fragiadakis (eds.)
Crete, Greece, 24-26 June 2019

INVERSE IDENTIFICATION OF BUFFETING AND SELF-EXCITED WIND LOADS ON THE HARDANGER BRIDGE FROM ACCELERATION DATA

Øyvind W. Petersen[1], Ole Øiseth[1], Torodd S. Nord[1] and E. Lourens[2]

[1] NTNU, Norwegian University of Science and Technology
7030 Trondheim, Norway
e-mail: {oyvind.w.petersen,ole.oiseth,torodd.nord}@ntnu.no

[2] Delft University of Technology
2628 CN Delft, The Netherlands
e-mail: e.lourens@tudelft.nl

Keywords: suspension bridge, structural monitoring, force identification, Kalman filter.

Abstract. *The traditional wind load assessment for long-span bridges rely on assumed models for the wind field and aerodynamic coefficients from wind tunnel tests, which usually introduces some uncertainties. It is therefore desired to develop tools that can utilize full-scale vibration response data from existing bridges in order to study the wind loading in detail for in-situ conditions. This paper presents a novel case study of inverse identification of dynamic wind loads on the 1310 m long Hardanger bridge, a suspension bridge equipped with a network of accelerometers. The identification method used is recent a unscented Kalman-type filter for joint input, state, and parameter estimation. A system model considering the still-air modes in addition to a quasi-steady submodel for the self-excited forces of the bridge is presented. Herein, the aerodynamic lift and pitch parameters are considered unknown and are jointly estimated with the buffeting forces. (...)*

1 INTRODUCTION

For very long and slender bridges, aerodynamic performance often becomes the critical factor in the reliable design [1]. Hence, it is important to understand the dynamic response behavior under wind excitation. In this arena, it is commonly accepted that the theories behind buffeting forces due to turbulence [2] and self-excited forces induced by the motion of structure [3] are governing. In addition to this comes static wind pressures and vortex-shedding [4, 5], but these are not the focus of this contribution. The calculation of the buffeting and self-excited involves the use of aerodynamic coefficients or functions, which in today's practice often are obtained from series of wind tunnel tests. Alternatively, simulations based on computational fluid dynamics can be performed [6, 7], with the drawback of requiring immense computational power. The numerical and small-scale experiments involve some uncertainties and simplifications, and sometimes it can be beneficial to learn directly from the existing bridges in their operating environment.

In recent years, the focus on structural health monitoring (SHM) have given engineers abundance of full-scale data from long-span bridges. This full-scale data can be valuable since it contains information the behavior of the bridge in the complex conditions that occurs in reality. It is therefore desired to use such data to explore the ability for testing and validation of the models for the wind loading and aerodynamic interaction. This can be a difficult task since the application of advanced signal processing methods can be encounter some trouble due to uncertain or non-idealized conditions, disturbances, and data from limited sensors.

One available tool to reduce the uncertainties in the dynamic behavior of structures is the use of inverse force identification methodologies in which the excitation forces, considered unknown, are estimated from limited (acceleration) response measurements. Although many techniques have been proposed in the literature [], the application of these inverse methods are not well-explored for large bridges. There is therefore a need to test the available methods to get experience on the performance.

In this work, the apply the novel input and state estimator in [8], which is a generalized version of earlier algorithms [9, 10]. This Kalman-type algorithm can be implemented in an unscented scheme, and allows for an extension to estimation of unknown system parameters. The method is tested for measurement data from a long-span suspension bridge. In the presented framework, the states are the modal responses, the unknown inputs are the buffeting forces and the uncertain parameters are quasi-steady coefficients related to the self-excitation of the bridge box girder under wind loading.

2 THEORY

2.1 Equations for the wind-induced dynamic response

This section derives a state-space formulation for the bridge dynamics, taking into account a quasi-steady form of self-excitation leading to aerodynamic stiffness and damping. We assume the following equations of motion in a FE-format for the response $\mathbf{u}(t) \in \mathbb{R}^{\mathrm{n_{DOF}}}$:

$$\mathbf{M}_0\ddot{\mathbf{u}}(t) + \mathbf{C}_0\dot{\mathbf{u}}(t) + \mathbf{K}_0\mathbf{u}(t) = \mathbf{f}_{\mathrm{b}}(t) + \mathbf{f}_{\mathrm{se}}(t) \tag{1}$$

where $\mathbf{f}_{\mathrm{b}}(t)$ are the buffeting forces and $(\cdot)_0$ denotes still-air properties. The self-excited forces $\mathbf{f}_{\mathrm{se}}(t)$ depend on the displacement and velocity motion of the structure, and is dealt with later in this section. A modal truncation ($\mathbf{u}(t) = \mathbf{\Phi}\mathbf{z}(t)$) yields the reduced-order representation for the

modal coordinate vector $\mathbf{z}(t) \in \mathbb{R}^{\mathrm{n_m}}$:

$$\ddot{\mathbf{z}}(t) + 2\boldsymbol{\Xi}\boldsymbol{\Omega}\dot{\mathbf{z}}(t) + \boldsymbol{\Omega}^2\mathbf{z}(t) = \boldsymbol{\Phi}^{\mathrm{T}}\mathbf{f}_{\mathrm{b}}(t) + \boldsymbol{\Phi}^{\mathrm{T}}\mathbf{f}_{\mathrm{se}}(t) \tag{2}$$

$\boldsymbol{\Omega}$ and $\boldsymbol{\Xi} \in \mathbb{R}^{\mathrm{n_m}}$ are diagonal matrices that contain the still-air natural frequencies and damping ratios. By introducing the modal state variable $\mathbf{x}(t) = [\mathbf{z}(t)^{\mathrm{T}} \quad \dot{\mathbf{z}}(t)^{\mathrm{T}}]^{\mathrm{T}} \in \mathbb{R}^{2\mathrm{n_m}}$, Eq. 2 can be cast into state-space form. Furthermore, the force vector $\mathbf{f}_{\mathrm{se}}(t)$ is set equal to $\mathbf{H}_{\mathrm{se,d}}(t,\boldsymbol{\epsilon})\boldsymbol{\Phi}\mathbf{z}(t) + \mathbf{H}_{\mathrm{se,v}}(t,\boldsymbol{\epsilon})\boldsymbol{\Phi}\dot{\mathbf{z}}(t)$, a transformation that is explained later. The time-evolution of the system then becomes:

$$\dot{\mathbf{x}}(t) = \Big(\begin{bmatrix} \mathbf{0} & \mathbf{I} \\ -\boldsymbol{\Omega}^2 & -2\boldsymbol{\Xi}\boldsymbol{\Omega} \end{bmatrix} + \begin{bmatrix} \mathbf{0} & \mathbf{0} \\ \boldsymbol{\Phi}^{\mathrm{T}}\mathbf{H}_{\mathrm{se,d}}(t,\boldsymbol{\epsilon})\boldsymbol{\Phi} & \boldsymbol{\Phi}^{\mathrm{T}}\mathbf{H}_{\mathrm{se,v}}(t,\boldsymbol{\epsilon})\boldsymbol{\Phi} \end{bmatrix} \Big)\mathbf{x}(t) + \begin{bmatrix} \mathbf{0} \\ \mathbf{I} \end{bmatrix} \boldsymbol{\Phi}^{\mathrm{T}}\mathbf{f}_{\mathrm{b}}(t) \tag{3}$$

or in compact notation:

$$\dot{\mathbf{x}}(t) = \mathbf{A}_{\mathrm{c}}(t,\boldsymbol{\epsilon})\mathbf{x}(t) + \mathbf{B}_{\mathrm{c}}\boldsymbol{\Phi}^{\mathrm{T}}\mathbf{f}_{\mathrm{b}}(t) \tag{4}$$

It is noted this results in a system which is linear, but time variant. When considering acceleration and displacement measurements, the output vector become:

$$\mathbf{y}(t) = \mathbf{S}_{\mathrm{a}}\ddot{\mathbf{u}}(t) + \mathbf{S}_{\mathrm{d}}\mathbf{u}(t) = \mathbf{G}_{\mathrm{c}}(t,\boldsymbol{\epsilon})\mathbf{x}(t) + \mathbf{J}_{\mathrm{c}}\boldsymbol{\Phi}^{\mathrm{T}}\mathbf{f}_{\mathrm{b}}(t) \tag{5}$$

with corresponding matrices:

$$\mathbf{G}_{\mathrm{c}}(t,\boldsymbol{\epsilon}) = \mathbf{S}_{\mathrm{a}}\boldsymbol{\Phi}\begin{bmatrix} -\boldsymbol{\Omega}^2 & -2\boldsymbol{\Xi}\boldsymbol{\Omega} \end{bmatrix} + \begin{bmatrix} \mathbf{S}_{\mathrm{d}}\boldsymbol{\Phi} & \mathbf{0} \end{bmatrix} + \mathbf{S}_{\mathrm{a}}\boldsymbol{\Phi}\begin{bmatrix} \boldsymbol{\Phi}^{\mathrm{T}}\mathbf{H}_{\mathrm{se,d}}(t,\boldsymbol{\epsilon})\boldsymbol{\Phi} & \boldsymbol{\Phi}^{\mathrm{T}}\mathbf{H}_{\mathrm{se,v}}(t,\boldsymbol{\epsilon})\boldsymbol{\Phi} \end{bmatrix} \tag{6}$$

$$\mathbf{J}_{\mathrm{c}} = \mathbf{S}_{\mathrm{a}}\boldsymbol{\Phi} \tag{7}$$

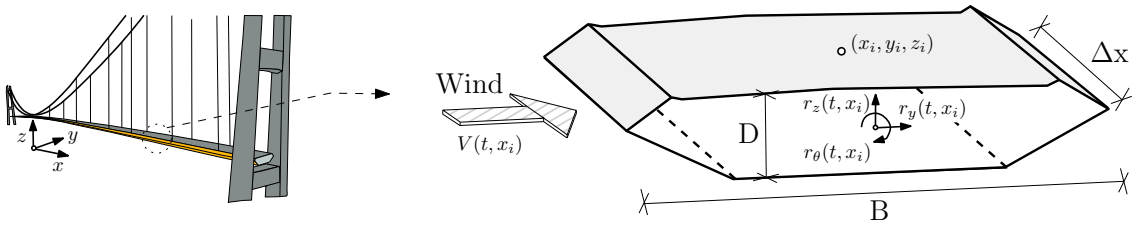

Figure 1: Suspension bridge and motion vectors of a segment of the box girder subjected to wind.

Next, the self-excited forces on the box girder are discussed. Although many model formulations are available [11], a simple memory-less model is adopted in this study for reasons of simplicity, implying the self-excited forces depend only on the structural displacement and velocity in the same time instant. Specifically, we employ a model called modified quasi-steady theory [12]. With reference to Fig. 1, the localized self-excited forces on a slice of the box girder with coordinate x_i are given on the form:

$$\begin{bmatrix} f_{\mathrm{se},y} \\ f_{\mathrm{se},z} \\ f_{\mathrm{se},\theta} \end{bmatrix} = \frac{1}{2}\rho V^2 B \Delta x \Big(\begin{bmatrix} p_4\frac{1}{B} & p_6\frac{1}{B} & p_3 \\ h_6\frac{1}{B} & h_4\frac{1}{B} & h_3 \\ a_6 & a_4 & a_3 B \end{bmatrix} \begin{bmatrix} r_y \\ r_z \\ r_\theta \end{bmatrix} + \begin{bmatrix} p_1\frac{1}{V} & p_5\frac{1}{V} & p_2\frac{B}{V} \\ h_5\frac{1}{V} & h_1\frac{1}{V} & h_2\frac{B}{V} \\ a_5\frac{B}{V} & a_1\frac{B}{V} & a_2\frac{B^2}{V} \end{bmatrix} \begin{bmatrix} \dot{r}_y \\ \dot{r}_z \\ \dot{r}_\theta \end{bmatrix} \Big) \tag{8}$$

or in compact notation:

$$\mathbf{f}_{\mathrm{se}}(t, x_i) = \mathbf{H}_{\mathrm{d}}(t, x_i, \boldsymbol{\epsilon})\mathbf{r}(t, x_i) + \mathbf{H}_{\mathrm{v}}(t, x_i, \boldsymbol{\epsilon})\dot{\mathbf{r}}(t, x_i) \tag{9}$$

where the parameter set $\boldsymbol{\epsilon} = [a_1 \dots a_6 \quad h_1 \dots h_6 \quad p_1 \dots p_6]^{\mathrm{T}}$ consist of 18 quasi-steady coefficients. This corresponds to modeling the aerodynamic derivatives as functions proportional to $\frac{B\omega}{V}$ or $(\frac{B\omega}{V})^2$ [12]. In the presented framework, the mean wind velocity $V(t, x_i)$ is allowed to vary with time, although the notation V is used for brevity. The span is divided into M equally spaced nodal points with coordinates $\{x_1, \dots, x_M\}$. Using matrices $\mathbf{S}_i \in \mathbb{R}^{3\times \mathrm{n_{DOF}}}$ to select $\mathbf{r}(t, x_i)$ from the larger vector $\mathbf{u}(t)$, the vector $\mathbf{f}_{\mathrm{se}}(t)$ in Eq. 1 now is taken as the lumped sum of contributions from all M nodes:

$$\begin{aligned}
\mathbf{f}_{\mathrm{se}}(t) = \sum_{i=1}^{M} \mathbf{S}_i^{\mathrm{T}} \mathbf{f}_{\mathrm{se}}(t, x_i) &= \sum_{i=1}^{M} \mathbf{S}_i^{\mathrm{T}} \big(\mathbf{H}_{\mathrm{d}}(t, x_i, \boldsymbol{\epsilon}) \mathbf{r}(t, x_i) + \mathbf{H}_{\mathrm{v}}(t, x_i, \boldsymbol{\epsilon}) \dot{\mathbf{r}}(t, x_i) \big) \\
&= \sum_{i=1}^{M} \mathbf{S}_i^{\mathrm{T}} \big(\mathbf{H}_{\mathrm{d}}(t, x_i, \boldsymbol{\epsilon}) \mathbf{S}_i \mathbf{u}(t) + \mathbf{H}_{\mathrm{v}}(t, x_i, \boldsymbol{\epsilon}) \mathbf{S}_i \dot{\mathbf{u}}(t) \big) \\
&= \sum_{i=1}^{M} \mathbf{S}_i^{\mathrm{T}} \mathbf{H}_{\mathrm{d}}(t, x_i, \boldsymbol{\epsilon}) \mathbf{S}_i \boldsymbol{\Phi} \mathbf{z}(t) + \sum_{i=1}^{M} \mathbf{S}_i^{\mathrm{T}} \mathbf{H}_{\mathrm{v}}(t, x_i, \boldsymbol{\epsilon}) \mathbf{S}_i \boldsymbol{\Phi} \dot{\mathbf{z}}(t) \\
&= \mathbf{H}_{\mathrm{se,d}}(t, \boldsymbol{\epsilon}) \boldsymbol{\Phi} \mathbf{z}(t) + \mathbf{H}_{\mathrm{se,v}}(t, \boldsymbol{\epsilon}) \boldsymbol{\Phi} \dot{\mathbf{z}}(t)
\end{aligned} \tag{10}$$

where the definitions of the (time and) parameter-dependent matrices $\mathbf{H}_{\mathrm{se,d}}(t, \boldsymbol{\epsilon})$ and $\mathbf{H}_{\mathrm{se,v}}(t, \boldsymbol{\epsilon}) \in \mathbb{R}^{\mathrm{n_{DOF}}\times \mathrm{n_{DOF}}}$ now are clear. A discretization in time ($t_k = k\Delta t$) of Eq. 4 and 5 now gives the following system equations:

$$\mathbf{x}_{k+1} = \mathbf{A}_{\mathrm{d}}(t_k, \boldsymbol{\epsilon}_k) \mathbf{x}_k + \mathbf{B}_{\mathrm{d}} \mathbf{p}_k \tag{11}$$

$$\mathbf{y}_k = \mathbf{G}_{\mathrm{d}}(t_k, \boldsymbol{\epsilon}_k) \mathbf{x}_k + \mathbf{J}_{\mathrm{d}} \mathbf{p}_k \tag{12}$$

where the substitution $\mathbf{p}_k = \boldsymbol{\Phi}^{\mathrm{T}} \mathbf{f}_{\mathrm{b}}(t_k)$ define the buffeting loads in the modal space. No parametric model is introduced for the buffeting or the turbulence. Provided that the wind velocity, the parameters, and the modal buffeting loads were known, the system output response could be straightforwardly solved from Eq. 11 and 12 for some given initial conditions. However, these are all, except the wind velocity, treated as unknown quantities; the estimation methodology is discussed in the next section.

2.2 Equations for the identification problem

The goal is to jointly estimate the inputs, states and the parameters for this system. The parameters are augmented into the state vector, resulting in the following final model of the dynamics:

$$\begin{bmatrix} \mathbf{x}_{k+1} \\ \boldsymbol{\epsilon}_{k+1} \end{bmatrix} = \begin{bmatrix} \mathbf{A}_{\mathrm{d}}(t_k, \boldsymbol{\epsilon}_k) & \mathbf{0} \\ \mathbf{0} & \mathbf{I} \end{bmatrix} \begin{bmatrix} \mathbf{x}_k \\ \boldsymbol{\epsilon}_k \end{bmatrix} + \begin{bmatrix} \mathbf{B}_{\mathrm{d}} \\ \mathbf{0} \end{bmatrix} \mathbf{p}_k + \begin{bmatrix} \mathbf{w}_k \\ \boldsymbol{\mu}_k \end{bmatrix} \tag{13}$$

$$\mathbf{y}_k = \begin{bmatrix} \mathbf{G}_{\mathrm{d}}(t_k, \boldsymbol{\epsilon}_k) & \mathbf{0} \end{bmatrix} \begin{bmatrix} \mathbf{x}_k \\ \boldsymbol{\epsilon}_k \end{bmatrix} + \mathbf{J}_{\mathrm{d}} \mathbf{p}_k + \mathbf{v}_k \tag{14}$$

According to principles from Kalman filtering, this model includes stochastic white noise on the modal states ($\mathbf{w}_k$) and on the measurements ($\mathbf{v}_k$), as well as a fictitious driving term for the parameters ($\boldsymbol{\mu}_k$). These vectors are all assumed mutually uncorrelated, zero-mean and with covariance relations:

$$\mathbb{E}[\mathbf{w}_k \mathbf{w}_l^{\mathrm{T}}] = \mathbf{Q}_{\mathrm{w}}\, \delta_{kl}, \quad \mathbb{E}[\mathbf{v}_k \mathbf{v}_l^{\mathrm{T}}] = \mathbf{R}\, \delta_{kl}, \quad \mathbb{E}[\boldsymbol{\mu}_k \boldsymbol{\mu}_l^{\mathrm{T}}] = \mathbf{Q}_{\mu}\, \delta_{kl} \tag{15}$$

Figure 2: The Hardanger bridge (photo: Ø.W. Petersen/NTNU)

We apply a Kalman-type algorithm from [8], which is termed unscented minimum-variance unbiased (UMVU) joint input-state (JIS) estimation. Specifically, we have implemented the "additive noise"-version, meaning the noise terms in Eq. 13 and 14 are separate from the other terms, as is assumed here. This leads to a faster calculation, since the covariances in Eq. 15 are explicit and the noise vectors need not be augmented into the state vector for the calculation of the so-called sigma points.

Some necessary mathematical conditions for the estimation should be discussed. Firstly, $\text{rank}(\mathbf{J}_\text{d}) = \text{n}_\text{m}$ is required is order to identify all n_m modal forces [8]. This condition is fulfilled for the actual system model presented later in Section 3.1. As the system matrices changes with time, the observability should formally be checked according to the theory in reference [13] (...).

3 IMPLEMENTATION FOR THE HARDANGER BRIDGE

3.1 Data from the Hardanger bridge

The practical test of the methodology is applied to data from the Hardanger bridge, a suspension bridge shown in Fig. 2. In this study, the bridge is modelled with $\text{n}_\text{m} = 14$ vibration modes from a FE model [14, 15], called H1-H5, V1-V8 and T1. The shapes of these modes along the main span are shown in Fig. 3 together with the natural frequencies and damping ratios. As discussed in [15, 16], the number of modes in the reduced-order model for long-span bridges (in inverse estimation) is mainly limited by the necessary criteria $\text{rank}(\mathbf{J}_\text{d}) = \text{n}_\text{m}$; more acceleration sensors are needed to be able to identify more modal forces.

This bridge have 20 accelerometers for measuring the dynamic response, and eight anemometers that measures wind velocities in the main span [17]. The positions of the sensors are given in references [15, 17].

A measurement data set with duration 30 min ($\Delta t = 0.1$ s) is studied. The direction of the wind is approximately 20° off the bridge normal throughout this period. The span of the bridge is discretized into $M = 65$ points ($\Delta x \approx 20$ m). First, the mean wind velocity for the eight anemometer measurements is found by using 10 minute moving averages. Then, linear interpolation is used estimate the field $V(x,t)$ between the anemometers, resulting in the time-spatial distribution in Fig. 4. Inhomogeneous features in the wind field is not uncommon for this bridge location [18], and in this case an apparent trend of higher velocities for one part of the bridge is observed. Although robust testing for (non-)stationarity of time series generally

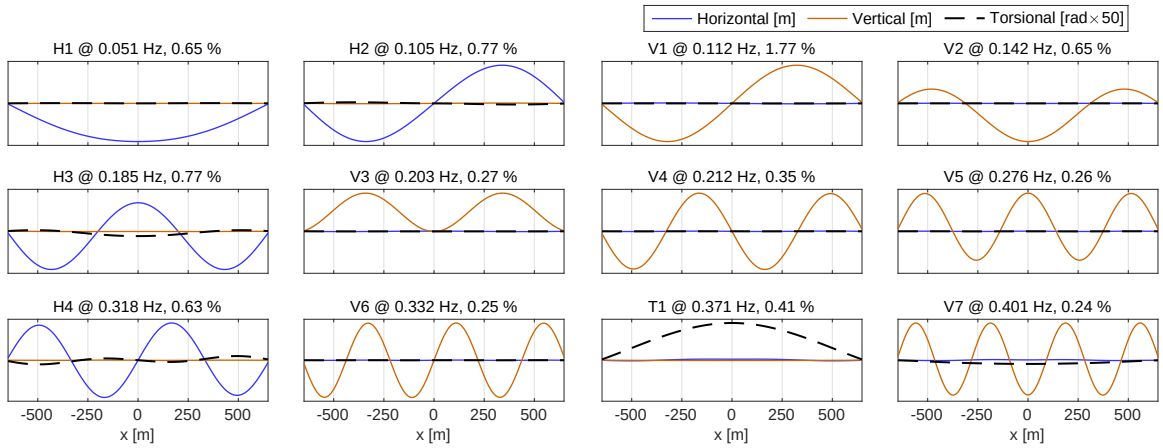

Figure 3: Horizontal, vertical and torsional deflection of the mode shapes along the main span.

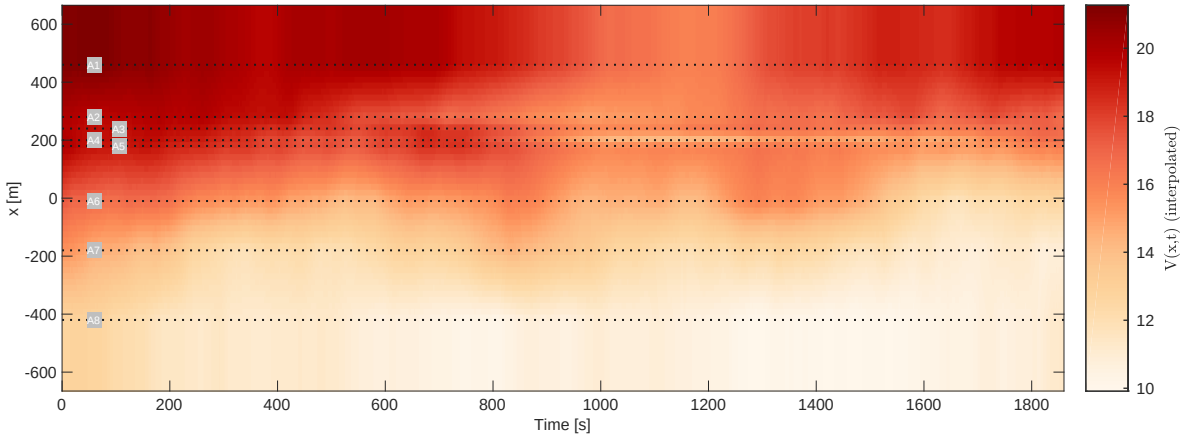

Figure 4: Estimated time-spatial distribution of the mean wind velocity along the main span. The horizontal lines indicate the positions of the anemometers A1-A8. Linear interpolation is used along the x-axis, with constant end values for extrapolation beyond A1 and A8.

is difficult, the mean wind velocity could intuitively also be said to have weakly non-stationary features for this 30 minute period. This is not a direct problem, however, as no stationarity assumptions are imposed on the loading or dynamic behavior in the UMVU-JIS estimation.

Some pre-processing of the response data is necessary. A low-pass filter is applied to mitigate the content below 0.5 Hz. A subset of the acceleration response data is shown in Fig. 5 for sensors in the quarter span. In addition to the acceleration data, displacements in the form of (offline) integrated accelerations are also included in the output vector to avoid instabilities in the estimation. This also involves high-passing the displacement data at 0.01 Hz.

3.2 Unscented estimation of inputs, states and parameters

Some initial values for the unknown quantities are also needed for the first time step in the algorithm. As the conditions at time t_0 are not practically determinable, the initial guess is set to $\mathbf{x}_0, \boldsymbol{\epsilon}_0, \mathbf{p}_0 = \mathbf{0}$. The error corresponding covariances are set to $\mathbf{P}_0^{\mathbf{x}} = \mathbf{I}$, $\mathbf{P}_0^{\boldsymbol{\mu}} = \mathbf{I}$, $\mathbf{P}_0^{\mathbf{p}} = \mathbf{I}$.

After some trials, it was found that estimation of all 18 parameters lead to some unrealistic

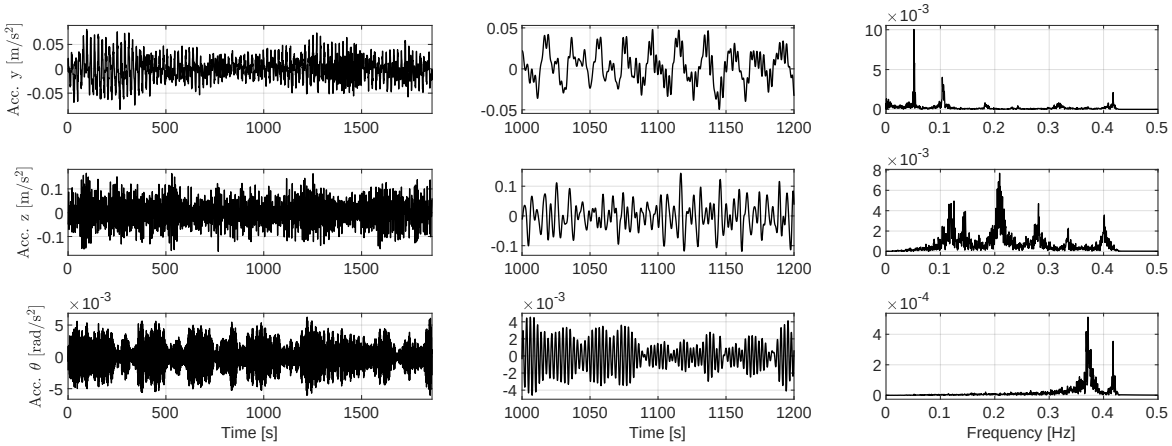

Figure 5: Acceleration response in the quarter span for the horizontal, vertical and torsional motions.

results, mostly connected to the self-excited drag effects (i.e., related to the motion in the y-direction). It was therefore chosen to reduce the parameter set to $a_1 - a_4$ and $h_1 - h_4$ (i.e., the vertical-torsional coupling in Eq. 8). For this type of bridge, it is well-known that these eight self-excitation coefficients are important for flutter analysis, and that the self-excited drag is usually not very large for streamlined cross sections. In accordance with [12], the remaining parameters were therefore set to fixed values:

$$\begin{aligned} &a_5 = -2\bar{C}_M, \;\; a_6 = 0, \;\; h_5 = -2\bar{C}_L, \;\; h_6 = 0 \\ &p_1 = -2\bar{C}_D\frac{D}{B}, \;\; p_2 = 0, \;\; p_3 = C'_D\frac{D}{B}, \;\; p_4 = 0, \;\; p_5 = (\bar{C}_L - C'_D\frac{D}{B}), \;\; p_6 = 0 \end{aligned} \tag{16}$$

where the following static force coefficients from wind tunnel tests are used [19]:

$$\begin{aligned} &\bar{C}_D = 1.05, \; C'_D = 0, \;\; \bar{C}_L = -0.363, \;\; C'_L = 2.22, \;\; \bar{C}_M = -0.017, \;\; \bar{C}'_M = 0.786 \\ &B = 18.3\,\text{m}, \;\; D = 3.25\,\text{m} \end{aligned} \tag{17}$$

An important aspect of the estimation is the choice of covariance matrices (Eq. 15). As noted in [8], the covariance magnitudes (noise levels) could influence the results quite considerably. $\mathbf{R} = 10^{-6}\,\mathbf{I}$ is used, a level which corresponds to $1 - 5\%$ of the output data standard deviations. For the process noise, $\mathbf{Q}_\text{w} = 10^{-2}\,\mathbf{I}$ is set. For the parameter covariance $\mathbf{Q}_\mu = c_\mu\,\mathbf{I}$, the three scalar values $c_\mu = 10^{-4}$, 10^{-6}, 10^{-8} and are tested, which are much less than the expected parameter order.

The identified modal forces are shown in 6 in the frequency-domain by a fast Fourier transform (FFT) of the time series. The value of $\mathbf{Q}_\mu$ does not really influence identified forces, therefore only a single solution is shown. Characteristic to ill-conditioned problems, identification of forces generally suffer from sensitivity in the solution to errors on the model or the output data. A known practical problem is that a few so-called cable-modes that could not be included in the state-space model in reality has a small contribution to the dynamic response in the box girder [16]. This leads to some unfortunate effects visible in Fig. 6, namely a spurious contribution around the frequencies 0.24, 0.37 and 0.41 Hz in the horizontal modes. Other than this, the modal forces appear to realistically resemble the frequency-domain characteristics of buffeting forces due to turbulence.

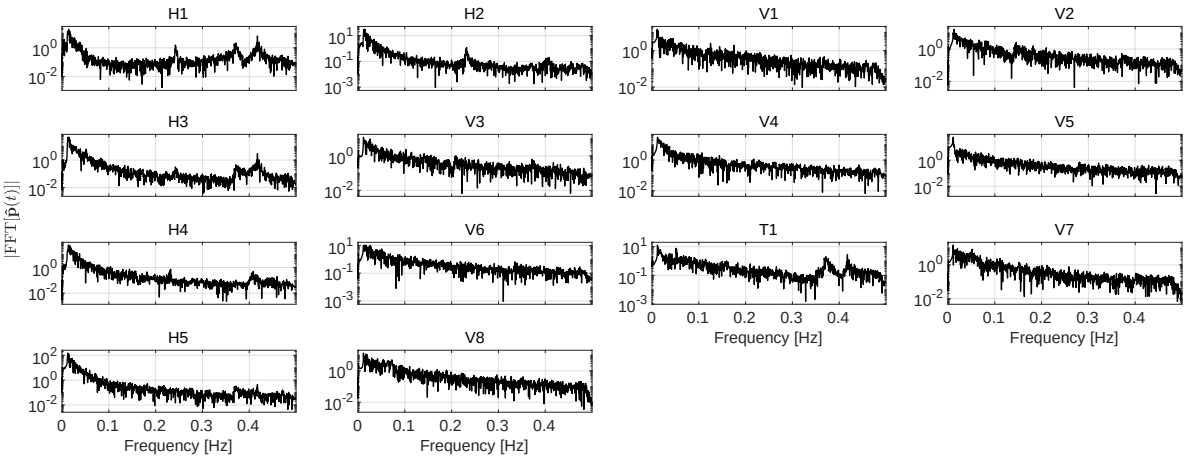

Figure 6: Estimated modal forces in the frequency-domain.

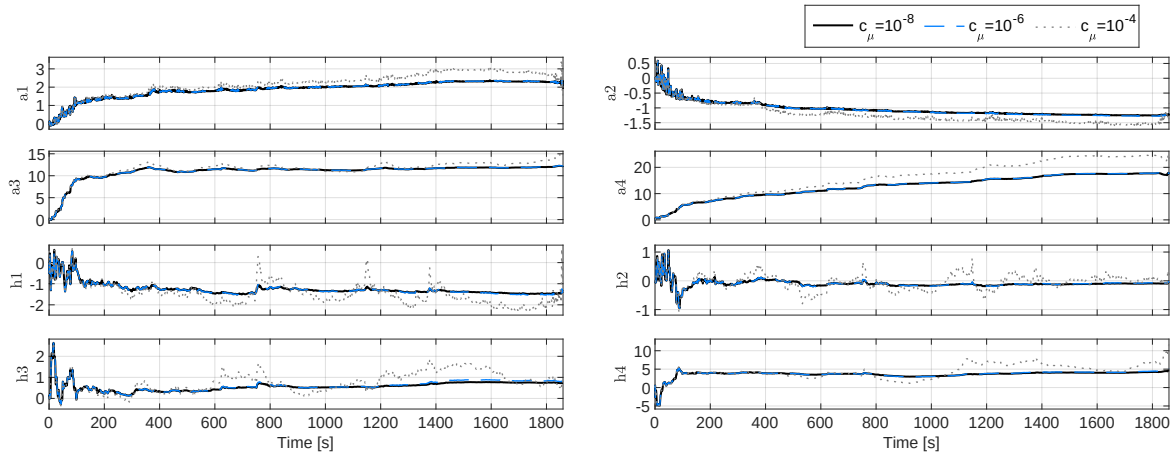

Figure 7: Estimated quasi-steady parameters.

Next, the attention is shifted to the parameter estimation. The parameter estimation is shown in Fig. 7. It is seen that for $c_\mu = 10^{-4}$, the dynamic response or loading tend to bleed into the parameter estimate, thus $c_\mu = 10^{-6}$ or $c_\mu = 10^{-8}$ is deemed a more suitable choice. It is expected that the parameters should be quite constant, but small time-variations could happen for changes in environmental conditions such as the wind yaw angle or mean the angle of attack. Although no formal convergence is achievable in unscented estimation, most parameters reach a relatively stable level after the initial 200 s. This is not the case for a_4 , which tend to slowly rise throughout the time period. A potential problem here is parameter magnitude differences, for which a shared c_μ-value introduces some compromise. The interpretation of the results should also factor in the individual parameter influence on the system dynamics. Generally, it is expected the most influential parameters for the system response are most accurately estimated, whereas parameters with a smaller influence could be more inaccurate since its deviations do not to the same degree affect the goodness of fit for the solution to the data. A sensitivity analysis could give some indications of the significance to trim out non-essential parameters.

A more intuitive way to assess the results is to study the effective natural frequencies and damping ratios of the system for the in-wind conditions. These can be solved from the eigen-

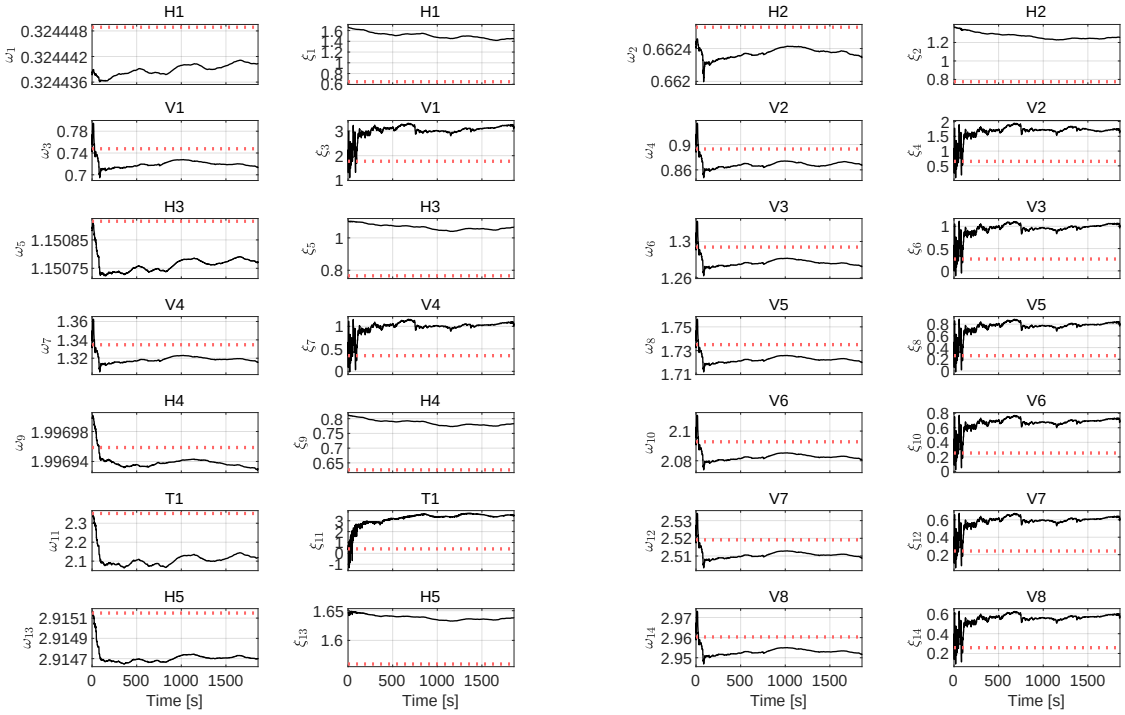

Figure 8: Evolution of natural frequencies (ω in rad/s) and damping ratios (ξ in %). The red lines indicate the still-air modal properties.

values of $\mathbf{A}_{\mathrm{c}}(t, \boldsymbol{\epsilon})$, which are on the form $\lambda_j = -\xi_j\omega_j \pm i\omega_j\sqrt{1-\xi_j^2}$. The modal properties will be time-varying since they are dependent on the mean wind velocity and the quasi-steady parameters, and Fig. 8 shows the evolution. Herein, it is the vertical and torsional modes that are most interesting, as changes in the horizontal modes mainly are driven by the assigned a priori values in Eq. 16. As expected, the effective damping ratios increases for all the modes compared to the still-air properties. In particular mode 11, the first torsion mode, has a strong shift in the natural frequency ($\sim 11\%$ reduction).

The use of advanced computational methodology to full-scale bridge data always has some uncertainties that are difficult to eliminate. In this context, the following sources could be mentioned:

- Limited anemometer data leads to uncertainties in the interpolated wind field $V(x,t)$.
- A number of uncertainties can be related to the UMVU-JIS estimation itself. Herein, the Kalman-type algorithms always have an estimate error uncertainty inherited from the white noise modelling. As shown, the noise covariance matrices influence to some degree the solution.
- Errors in the FE-based state-space model could give some incorrect estimates. Although the model is tuned [14], some temperature variations could affect the still-air natural frequencies and damping and thus also slightly the graphs in Fig. 8.
- The self-excitation of the cables could give some damping contributions. If the wind velocity at the elevation of the main cable was known, formulas similar to Eq. 8 could

be included for the self-excitation of the main cable by letting its drag coefficient be an unknown parameter.

- Local traffic could give some small dynamic response contributions to the considered modes.

4 CONCLUSIONS

The wind-induced dynamic response is an important but often uncertain aspect of long-span bridges due to uncertainties in the models for wind load prediction. This paper has presented a framework for state-space modelling of long-span bridges, taking into account the self-excited forces for the vertical and torsional modes through a set of modified quasi-steady parameters. Using recently developed unscented Kalman-type estimation schemes, this model can be applied for coupled input-state-parameter estimation to dynamic response measurements from bridges with monitoring systems.

The methodology is tested to acceleration from the Hardanger bridge, which is modelled using 14 modes. The identified forces have the characteristics of buffeting forces. Most estimated parameters reach a stable values. Although the estimated parameters are still are uncertain, it is shown they do provide realistic changes in the effective modal properties such as increased damping.

REFERENCES

[1] A. Larsen. Aerodynamic aspects of the final design of the 1624 m suspension bridge across the Great Belt. *Journal of Wind Engineering and Industrial Aerodynamics*, 48 (2-3):261–285, 1993.

[2] R. Scanlan. The action of flexible bridges under wind, II: buffeting theory. *Journal of Sound and Vibration*, 60(2):201–211, 1978.

[3] R. Scanlan. The action of flexible bridges under wind, I: flutter theory. *Journal of Sound and Vibration*, 60(2):187–199, 1978.

[4] G. Diana, F. Resta, M. Belloli, and D. Rocchi. On the vortex shedding forcing on suspension bridge deck. *Journal of Wind Engineering and Industrial Aerodynamics*, 94(5): 341–363, 2006.

[5] T. Wu and A. Kareem. An overview of vortex-induced vibration (VIV) of bridge decks. *Frontiers of Structural and Civil Engineering*, 6(4):335–347, 2012.

[6] M. Sarwar, T. Ishihara, K. Shimada, Y. Yamasaki, and T. Ikeda. Prediction of aerodynamic characteristics of a box girder bridge section using the LES turbulence model. *Journal of Wind Engineering and Industrial Aerodynamics*, 96(10-11):1895–1911, 2008.

[7] T. A. Helgedagsrud, Y. Bazilevs, A. Korobenko, K. M. Mathisen, and O. A. Øiseth. Using ALE-VMS to compute aerodynamic derivatives of bridge sections. *Computers & Fluids*, 2018.

[8] W. Song. Generalized minimum variance unbiased joint input-state estimation and its unscented scheme for dynamic systems with direct feedthrough. *Mechanical Systems and Signal Processing*, 99:886–920, 2018.

[9] E. Lourens, C. Papadimitriou, S. Gillijns, E. Reynders, G. De Roeck, and G. Lombaert. Joint input-response estimation for structural systems based on reduced-order models and vibration data from a limited number of sensors. *Mechanical Systems and Signal Processing*, 29:310–327, 2012.

[10] S. Gillijns and B. De Moor. Unbiased minimum-variance input and state estimation for linear discrete-time systems with direct feedthrough. *Automatica*, 43(5):934–937, 2007.

[11] I. Kavrakov and G. Morgenthal. A comparative assessment of aerodynamic models for buffeting and flutter of long-span bridges. *Engineering*, 3(6):823–838, 2017.

[12] O. Øiseth, A. Rönnquist, and R. Sigbjörnsson. Simplified prediction of wind-induced response and stability limit of slender long-span suspension bridges, based on modified quasi-steady theory: a case study. *Journal of Wind Engineering and Industrial Aerodynamics*, 98(12):730–741, 2010.

[13] M. N. Chatzis, E. N. Chatzi, and A. W. Smyth. On the observability and identifiability of nonlinear structural and mechanical systems. *Structural Control and Health Monitoring*, 22(3):574–593, 2015.

[14] Ø. W. Petersen and O. Øiseth. Finite element model updating of a long span suspension bridge. In R. Rupakhety, S. Olafsson, and B. Bessason, editors, *Proceedings of the International Conference on Earthquake Engineering and Structural Dynamics*, pages 335–344. Springer International Publishing, 2019. ISBN 978-3-319-78187-7.

[15] Ø. W. Petersen, O. Øiseth, and E. Lourens. The use of inverse methods for response estimation of long-span suspension bridges with uncertain wind loading conditions. *Journal of Civil Structural Health Monitoring*, 9(1):21–36, 2019.

[16] Ø. W. Petersen, O. Øiseth, and E. Lourens. Investigation of dynamic wind loads on a long-span suspension bridge identified from measured acceleration data. *(submitted for journal publication)*, 2019.

[17] A. Fenerci, O. Øiseth, and A. Rønnquist. Long-term monitoring of wind field characteristics and dynamic response of a long-span suspension bridge in complex terrain. *Engineering Structures*, 147:269–284, 2017.

[18] T. M. Lystad, A. Fenerci, and O. Øiseth. Evaluation of mast measurements and wind tunnel terrain models to describe spatially variable wind field characteristics for long-span bridge design. *Journal of Wind Engineering and Industrial Aerodynamics*, 179:558–573, 2018.

[19] B. Siedziako, O. Øiseth, and A. Rønnquist. An enhanced forced vibration rig for wind tunnel testing of bridge deck section models in arbitrary motion. *Journal of Wind Engineering and Industrial Aerodynamics*, 164:152–163, 2017.